Positioning and Tracking of High-speed Trains with Non-linear State Model for 5G and Beyond Systems

Jukka Talvitie, Toni Levanen, Mike Koivisto and Mikko Valkama
Electrical Engineering, Tampere University, Finland
E-mail: jukka.talvitie@tuni.fi

***Abstract*—High-speed trains (HSTs) with fifth generation (5G) communications services, including both high rate data links and high reliability mission-critical services, are considered as one of the new industry verticals facilitated by the 5G connectivity. In this paper, we study positioning of HSTs in 5G new radio (NR) networks based on time difference of arrival (TDoA) and angle-of-arrival (AoA) measurements, obtained with specific 5G NR reference signals at the millimeter wave (mmWave) frequency. Moreover, the HST is tracked with an extended Kalman filter, where, instead of conventional linear state-transition model, we propose and derive a non-linear state-transition model, including the train position, absolute train velocity, and train heading. Furthermore, by introducing a state-dependent process variance for the angular velocity of the train, we show that the positioning performance of the HST can be significantly improved compared to the conventional linear state-transition modeling. Based on realistic simulations on a real-life high-speed track, we show that the proposed positioning engine can reach 95% percentile estimation accuracies of 2.3 m, 0.47 m/s, and 1.6 deg, for the train position, train velocity, and train heading, respectively, thus fulfilling the requirements specified by the 3GPP for machine control and transportation services.**

***Index Terms*—Positioning, Extended Kalman filter, EKF, Fifth generation mobile networks, 5G, New Radio, NR, High-speed trains, HST**

I. Introduction

The emerging fifth generation (5G) new radio (NR) networks are expected to enable services for a wide variety of industry verticals by providing high data rates via extreme broadband, machine type communications together with Internet of Things (IoT) applications, as well as Ultra-Reliable and Low-Latency Communication (URLLC) for mission-critical services. One of the envisioned 5G verticals is high-speed trains (HSTs) with enhanced communications capabilities, as discussed, for example, in [1]–[3]. Besides providing high data rate internet connectivity for the HSTs, 5G NR network can also offer significant support to railway management systems via URLLC and IoT technologies for increased efficiency and safety. Furthermore, 5G NR networks are able to accelerate the deployment rate of autonomous trains, and have potential to revolutionize future public transportation systems.

Positioning and tracking are considered as one of the most important features of the upcoming 5G NR networks [4], [5]. When considering railway systems, ultra reliable and close to real time train positioning, which is not attainable by global navigation satellite system (GNSS) based technologies alone, as discussed in [6], can improve railway safety, but also introduces performance gain for the underlying communications system via supplementary location-aware radio resource management (RRM) algorithms [7], [8]. Positioning in 5G networks has been earlier studied, for example, in [6], [9]–[11], where [6] focuses especially on the HST scenario. In order to achieve high-accuracy position estimates, time of arrival (ToA), time difference of arrival (TDoA) and angle-of-arrival (AoA) based measurements have been proposed together with proper device tracking methods. Since each of the above measurements is non-linearly mapped to the position coordinates, utilization of an extended Kalman filter (EKF) is preferred, as it enables a practically feasible tracking approach with a compatibility of non-linear models via a locally exploited linear approximation. However, the corresponding state-transition model, describing the characteristics of device mobility, is often considered as linear.

The conventional linear state-transition model, for example, used for the HST scenario in [6], incorporates the train x-coordinate and y-coordinate together with the corresponding train velocity components in x-direction and y-direction. However, with HSTs, as well as with many other vehicle types, a state-transition model with conventionally defined Cartesian velocity components, is not by default an optimum choice for tracking, as shown in this paper. Moreover, we propose modeling the HST mobility with polar velocity components, consisting of the heading angle and the absolute velocity of the train. This type of modeling is intuitive for a large mass HST, which has a limited acceleration capability and presumably a velocity-dependent turning radius. Also for other types of vehicles, including all marine vessels, all vehicles on wheels, and at least solid wing aerial vehicles, using of polar velocity components is reasonable, therefore increasing the value of the novel findings provided in this paper. Furthermore, the proposed approach introduces a state-dependent configuration of the variance of the angular velocity for enhanced positioning performance. Nonetheless, the proposed state-transition model with the vehicle heading and absolute velocity is non-linear, and thus, requires appropriate linearization according to the EKF principle.

In this paper, based on a simulation of a real-life high-speed railway track between Shanghai and Beijing in China, based on the data obtained from [12], we show that by using specified 5G NR reference signals at the millimeter wave (mmWave)

This work was partially supported by Finnish Foundation for Technology Promotion.

frequency, the proposed approach with a state-dependent mobility model covariance, is able to achieve 2.3 m accuracy with 95% probability. For this we derive the considered EKF state-transition models with the state-depedent covariance, and the corresponding measurement model including TDoA and AoA measurements. In addition, we analyze the positioning accuracies separately for different train mobility characteristics, including an accelerating train, a train with a constant cruising velocity, and a train standing still. Besides studying positioning accuracy, estimation of the train velocity and train heading are also considered, since they have a crucial role in many use cases in location-aware communications, such as Doppler compensation for high-speed communication links, studied in [7]. Overall, the results obtained in this paper indicate that the chosen state-transition model can have a substantial impact on the positioning performance, and thus, needs to be properly addressed in positioning studies for various verticals enabled by the 5G and beyond systems.

II. System Model and Positioning Measurements

A. System model and considered HST scenario

The deployment of the 5G NR network in the considered HST scenario follows the guidelines of 3rd generation partnership project (3GPP) specifications given in [3, Section 6.1.5] for the mmWave frequencies. The 5G NR network coverage is implemented by uniformly distributing remote radio-heads (RRHs) in both sides of the track with a fixed 580 m inter-site distance and 5 m distance to the track, as illustrated in Fig. 2. At each RRH there are two antenna panels in 45 degree angle with respect to the track for covering both track directions. Moreover, the network operates according to a single-frequency principle, where all RRHs operate simultaneously in the same frequency band at 30 GHz carrier frequency. On top of the train there is a relay node, which passes through all communications between the train and the network, including HST system management data and passenger data. The train side relay node is equipped with two antenna panels facing towards the nose and tail of the train.

In order to ensure that the train position information at the network side is reliable and up-to-date, the positioning approach considered in this paper is based on uplink signals, and thus, positioning measurements and position estimation are managed at the network side. Nonetheless, because the main contribution of this paper is concentrated on studying the train mobility model rather than the measurement model, considering downlink measurements is also applicable for the proposed methods. The positioning measurements at the RRHs are based on the 5G NR uplink sounding reference signal (SRS), specified in [13, Section 6.4.1.4]. Furthermore, the positioning measurements are obtained during a beam training process occurring at regular time-intervals, where the uplink and downlink beams are sweeped over all applicable angles. However, it is worth of noticing that the full beam sweep is not necessarily needed, but only an appropriate subset of beams, for example, based on the previously used beams or the estimated location.

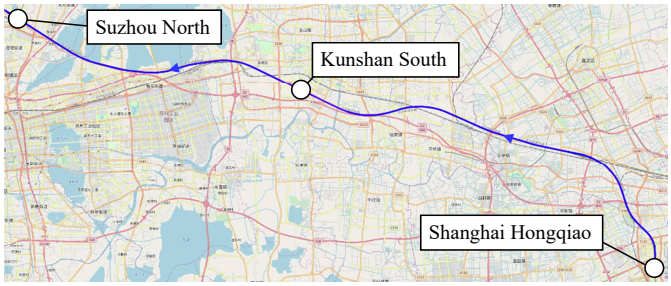

Fig. 1. The considered test track on the Shanghai-Beijing high-speed railway based on data obtained from [12].

For one pair of transmit and receive beams, the m^{th} received sample at the k^{th} RRH is given as

$$z_k[m] = \mathbf{g}_{\text{RX},k}\left(\gamma_k[m]\mathbf{\Lambda}_k[m]\mathbf{g}_{\text{TX}}u_{\text{SRS}}[m-\zeta_k] + \mathbf{n}_k[m]\right), \tag{1}$$

where $\mathbf{n}_k[m] \in \mathbb{C}^{N_{\text{RX}}}$ describes white Gaussian noise for each receiver antenna element, $\mathbf{g}_{\text{TX}} \in \mathbb{C}^{N_{\text{TX}}}$ and $\mathbf{g}_{\text{RX},k} \in \mathbb{C}^{N_{\text{RX}}}$ are the steering vectors for the transmit and the receive beams, respectively. Moreover, $\gamma[m]_k$ introduces the large scale channel characteristics including path loss and shadowing, and $\mathbf{\Lambda}_k[m]$ incorporates the effects of fast fading and Doppler spreading via a spatial power delay profile, which includes the line of sight (LoS) radio propagation path. In general, the channel modeling in this paper is implemented based on the 3GPP-specifications provided in [14], and more detailed information on the parameter configurations are presented with the simulation results in Section IV. Furthermore, in order to enable modeling of arbitrary time delays of received signals without any restrictions due to the used sampling rate, the m^{th} transmitted signal sample with a fractional sample delay is defined as

$$u_{\text{SRS}}[m-\zeta_k] = \sum_{q=0}^{N_{\text{SRS}}-1} u_{\text{SRS}}[q]\text{sinc}(m-q-\zeta_k), \tag{2}$$

where N_{SRS} is the number of samples in the transmitted signal u_{SRS}, and $\zeta_k = F_s\tau_k$ is the radio propagation delay given in fractional samples, where F_s is the sampling frequency and τ_k is the radio propagation delay for the LoS path of the k^{th} RRH. It is worth noticing that the effect of radio propagation delays for other observed radio paths are taken into account in the spatial channel matrix, where the propagation delays are defined with respect to the LoS path.

B. Positioning measurements

The positioning approach considered in this paper utilizes both the TDoA and the AoA measurements. Moreover, TDoA measurements enable high positioning accuracy, and they can be obtained without strict synchronization requirements between the network and the train. In addition, AoA measurements supplement the geometry of the measurement set, and they are straightforwardly accessible via inbuilt beam training processes included in mmWave systems.

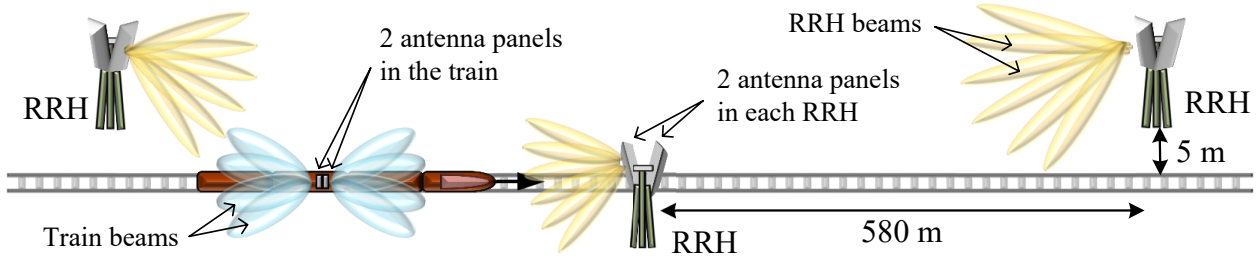

Fig. 2. Illustration of the considered high-speed railway scenario based on the guidelines specified in [3].

The TDoA measurements are obtained by acquiring the beam-wise cross-correlation between the received signal and the known SRS as

$$r_{k,i}[l] = \sum_{m=0}^{N_{\text{SRS}}-1} u^*_{\text{SRS}}[m-l] z_k[m], \tag{3}$$

where $r_{k,i}[l]$ is the cross-correlation function observed in the k^{th} RRH for the i^{th} receive beam. The set of beam-wise correlation functions is defined for one transmit beam, and thus, if multiple transmit beams are included in the beam training process, only the transmit beam with the highest received signal strength over all receive beams is considered. Furthermore, the propagation delay estimate at the k^{th} RRH can be determined based on the maximum observed absolute value of the correlation function as

$$\hat{l}_k = \arg\max_{l,i} |r_{k,i}[l]| \text{ and } \hat{\tau}_k = \frac{\hat{l}_k}{F_{\text{s}}}, \tag{4}$$

where F_{s} is the sampling frequency, and $\hat{l}_k$ and $\hat{\tau}_k$ are the estimated propagation delay in samples and in seconds, respectively. However, because of the clock error between the train and the network, $\hat{\tau}_k$ is only a pseudo-measurement according to the TDoA principle.

The AoA estimates are obtained based on the same cross-correlation function used with the timing measurements in (3), and the AoA estimate at the k^{th} RRH can be obtained as

$$\hat{\theta}_k[n] = \mathbf{w}_k^{\text{T}}[\theta_{k,1}, \theta_{k,2}, \ldots, \theta_{k,N_b}]^{\text{T}}, \tag{5}$$

where $\theta_{k,i}$ is the known direction of the i^{th} receive beam, and $\mathbf{w}_k = [w_{k,1}, w_{k,2}, \ldots, w_{k,N_b}]^{\text{T}}$, where

$$w_{k,i} = \frac{\hat{\xi}_{k,i}}{\sum_{j \in \Omega_{\text{largest}}} \hat{\xi}_{k,j}}, \quad \text{with} \quad \hat{\xi}_{k,i} = \max_l \tilde{r}_{k,i}[l], \tag{6}$$

where Ω_{largest} is the set of N_{largest} beam-indices that correspond to the largest correlation function values. In this paper, we define $N_{\text{largest}} = 3$ for the used AoA estimation approach.

III. Positioning Methods for High-Speed Trains

In this section, we first present the linear state model and the proposed non-linear state model of the considered EKF for modeling the HST mobility. After this, we describe the common update-step of the EKF utilizing the obtained TDoA and AoA measurements.

A. Linear State-Transition Model

The first state-transition model is a well-known nearly constant velocity model, utilized, for example, in [10], where the position of the train is estimated and tracked jointly with the Cartesian velocity components of the train. In this case, the state-vector can be defined as

$$\mathbf{s}[n] = [x[n], y[n], v_x[n], v_y[n]]^{\text{T}} \in \mathbb{R}^{4\times 1}, \tag{7}$$

where $x[n]$, $y[n]$, $v_x[n]$, and $v_y[n]$, are the x-coordinate and the y-coordinate of the train, and the Cartesian velocity components in the x-direction and the y-direction, respectively. In the nearly constant velocity model, the state model is linear and it can be written in a general form as

$$\mathbf{s}[n] = \mathbf{F}\mathbf{s}[n-1] + \mathbf{q}[n], \tag{8}$$

where $\mathbf{q}[n] \sim \mathcal{N}(0, \mathbf{Q}[n])$ is the zero-mean Gaussian process noise with the covariance matrix

$$\mathbf{Q}[n] = \sigma_{\text{a}}^2 \begin{bmatrix} \frac{\Delta t^3}{3}\mathbf{I}_{2\times 2} & \frac{\Delta t^2}{2}\mathbf{I}_{2\times 2} \\ \frac{\Delta t^2}{2}\mathbf{I}_{2\times 2} & \Delta t \mathbf{I}_{2\times 2} \end{bmatrix}, \tag{9}$$

and $\mathbf{F}$ is the linear state model matrix which is given as

$$\mathbf{F} = \begin{bmatrix} \mathbf{I}_{2\times 2} & \Delta t \cdot \mathbf{I}_{2\times 2} \\ \mathbf{0}_{2\times 2} & \mathbf{I}_{2\times 2} \end{bmatrix}. \tag{10}$$

Thereafter, the a priori estimates for the mean and covariance matrix can be obtained using the prediction step equations of the classical Kalman filter (KF) as

$$\hat{\mathbf{s}}^-[n] = \mathbf{F}\hat{\mathbf{s}}^+[n-1] \tag{11}$$

$$\hat{\mathbf{P}}^-[n] = \mathbf{F}\hat{\mathbf{P}}^+[n-1]\mathbf{F}^{\text{T}} + \mathbf{Q}[n], \tag{12}$$

where $\hat{\mathbf{s}}^+[n-1]$ and $\hat{\mathbf{P}}^+[n-1]$ are the previous step a posteriori estimates of the mean and covariance, respectively.

B. Non-Linear State-Transition Model

The second considered state-transition model consists of tracking not only the position of the train but also the heading angle and the speed of the train. Hence, the state-vector $\mathbf{s}[n]$ of the system at some time-instant n is given as

$$\mathbf{s}[n] = [x[n], y[n], v[n], h[n]]^{\text{T}} \in \mathbb{R}^{4\times 1}, \tag{13}$$

where $x[n]$, $y[n]$, $v[n]$, and $h[n]$ are the x-coordinate and the y-coordinate, the speed, and the heading angle of the train,

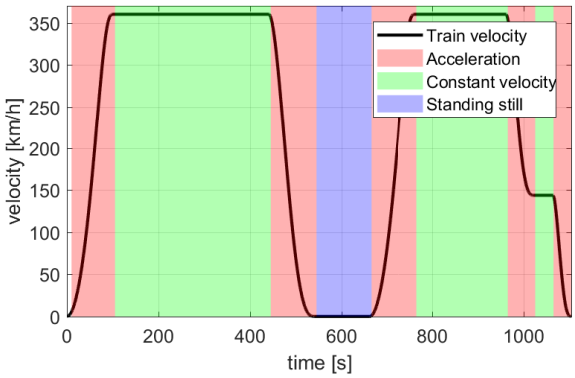

Fig. 3. Considered HST velocity over the track along with the parts of the track with different mobility characteristics.

respectively. Since the transition of the train's position between two consecutive time-instants depends on the heading angle and the speed of the train, the considered state model can be written in a general form as

$$\mathbf{s}[n] = \mathbf{f}(\mathbf{s}[n-1]) + \mathbf{q}[n], \tag{14}$$

where $\mathbf{f}(\cdot)$ is the non-linear state-transition model and it is given as

$$\mathbf{f}(\mathbf{s}[n-1]) = \begin{bmatrix} x[n-1] + \Delta t v[n-1]\cos(h[n-1]) \\ y[n-1] + \Delta t v[n-1]\sin(h[n-1]) \\ v[n-1] \\ h[n-1] \end{bmatrix}, \tag{15}$$

where Δt denotes a time-interval between the consecutive time-instants. Moreover, $\mathbf{q}[n] \sim \mathcal{N}(0, \mathbf{Q}[n])$ denotes the zero-mean Gaussian process noise of the state model.

In order to obtain the new a priori estimates for the mean $\hat{\mathbf{s}}^-[n]$ and covariance $\hat{\mathbf{P}}^-[n]$, the previous a posteriori estimates $\hat{\mathbf{s}}^+[n-1]$ and $\hat{\mathbf{P}}^+[n-1]$ are propagated through the prediction step equations of an EKF, which can be given in a general form as

$$\hat{\mathbf{s}}^-[n] = \mathbf{f}(\hat{\mathbf{s}}^+[n-1]) \tag{16}$$

$$\hat{\mathbf{P}}^-[n] = \mathbf{F}[n]\hat{\mathbf{P}}^+[n-1]\mathbf{F}[n]^{\mathrm{T}} + \mathbf{Q}[n], \tag{17}$$

where $\mathbf{F}[n]$ is the Jacobian matrix of the considered non-linear state model function $\mathbf{f}(\cdot)$ evaluated at the a posteriori mean $\hat{\mathbf{s}}^+[n-1]$. Given the state model function (15), the Jacobian matrix $\mathbf{F}[n]$ in (17) can be written as

$$\mathbf{F}[n] = \begin{bmatrix} \mathbf{I}_{2\times 2} & \Delta t \cdot \tilde{\mathbf{F}}[n] \\ \mathbf{0}_{2\times 2} & \mathbf{I}_{2\times 2} \end{bmatrix}, \tag{18}$$

where the sub-matrix $\tilde{\mathbf{F}}[n] \in \mathbb{R}^{2\times 2}$ is given by

$$\tilde{\mathbf{F}}[n] = \begin{bmatrix} \cos(\hat{h}^+[n-1]) & -\hat{v}^+[n-1]\sin(\hat{h}^+[n-1]) \\ \sin(\hat{h}^+[n-1]) & \hat{v}^+[n-1]\cos(\hat{h}^+[n-1]) \end{bmatrix}. \tag{19}$$

TABLE I
CONSIDERED SIMULATION PARAMETERS

Parameter	Value
Carrier frequency	30 GHz
Channel bandwidth	400 MHz
Subcarrier spacing	120 kHz
Path loss model	urban micro (UMi)
Fast fading model	clustered delay line D (CDL-D)
Delay spread	100 ns
RRH antenna array size	8 x 4 (hor. x ver.)
Train antenna array size	4 x 4 (hor. x ver.)
Transmission power	30 dBm
Inter-RRH distance	580 m
EKF step interval	100 ms
Max. num. of observed RRHs	5
EKF angular velocity std.	$\sigma_\omega[n] = \frac{1}{10000}\exp(\frac{\lvert\hat{v}[n]\rvert}{20})$
EKF acceleration std.	$\sigma_a = 3$

Since the state-transition of the system is driven by the noise in the acceleration and in the angular velocity, the process noise covariance matrix $\mathbf{Q}[n]$ of the state-transition model (17) can be written as [15]

$$\mathbf{Q}[n] = \mathbf{G}(\hat{\mathbf{s}}^+[n-1])\tilde{\mathbf{Q}}[n]\mathbf{G}(\hat{\mathbf{s}}^+[n-1])^{\mathrm{T}}, \tag{20}$$

where $\tilde{\mathbf{Q}}[n] = \mathrm{diag}(\sigma_a^2, \sigma_\omega^2[n])$, and $\mathbf{G}(\hat{\mathbf{s}}^+[n-1]) \in \mathbb{R}^{4\times 2}$ is given as

$$\mathbf{G}[n] = \begin{bmatrix} \frac{\Delta t^2}{2}\cos(\hat{h}^+[n-1]) & 0 \\ \frac{\Delta t^2}{2}\sin(\hat{h}^+[n-1]) & 0 \\ \Delta t \cdot \mathbf{I}_2 \end{bmatrix}. \tag{21}$$

Whereas the variance of the acceleration noise of the process is assumed to be fixed, the variance of the angular velocity is defined as state-dependent, which allows configuring process dynamics according to the estimated process state. In this paper, $\sigma_\omega^2[n]$ is altered based on the estimated train velocity at each state. For example, with a low estimated train velocity, it is more likely to have also a low angular velocity. Moreover, when the train is standing still, it is sensible to consider a fixed heading. Nonetheless, the exact mapping between the estimated velocity $\hat{v}[n]$ (i.e., the third element of $\hat{\mathbf{s}}^-[n]$ in (11)) and $\sigma_\omega[n]$ is evaluated by exploiting the available statistics related to the observed velocity and angular velocity over the considered track. As a result, an explicit mapping between the $\hat{v}[n]$ and $\sigma_\omega[n]$ is obtained as given in Table I.

C. Common Update-Phase for Both State-Models

A non-linear measurement model that relates the state of the system to the available measurements $\mathbf{y}[n]$ can be written as

$$\mathbf{y}[n] = \mathbf{h}(\mathbf{s}[n]) + \mathbf{r}[n], \tag{22}$$

where $\mathbf{h}(\cdot)$ is the non-linear measurement model function, and $\mathbf{r}[n] \sim \mathcal{N}(0, \mathbf{R}[n])$ is the measurement noise vector. Now, the measurement vector $\mathbf{y}[n]$ consists of both AoA and TDoA measurements and therefore, it can be written as

$$\begin{aligned} \mathbf{y}[n] &= [\hat{\boldsymbol{\theta}}[n]^{\mathrm{T}}, \Delta\hat{\boldsymbol{\tau}}[n]^{\mathrm{T}}]^{\mathrm{T}} \\ &= [\hat{\theta}_1[n], \ldots, \hat{\theta}_{N_{\mathrm{RRH}}}[n], \Delta\hat{\tau}_1[n], \ldots, \Delta\hat{\tau}_{N_{\mathrm{RRH}}-1}[n]]^{\mathrm{T}}. \end{aligned} \tag{23}$$

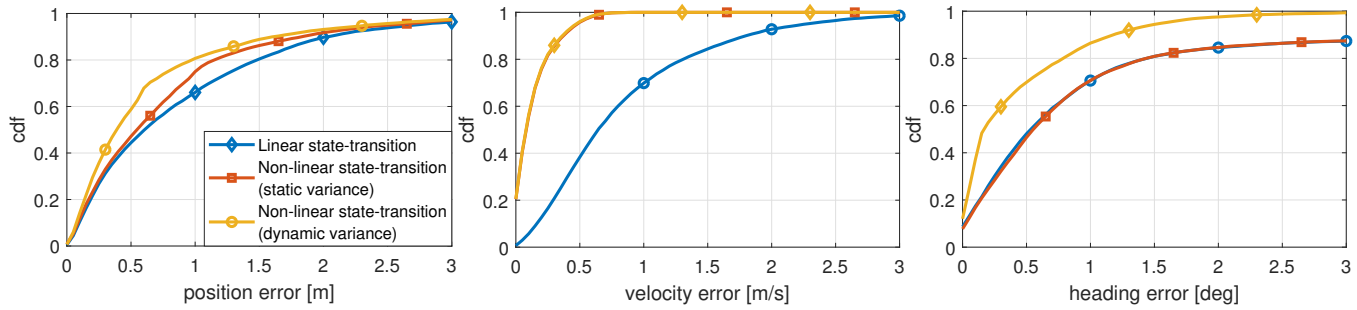

Fig. 4. Cumulative estimation errors over the whole track for train position, train velocity, and train heading, with the linear state-transition model, and the non-linear state-transition model

Consequently, the corresponding measurement model function can be written as $\mathbf{h}(\mathbf{s}[n]) = [\mathbf{h}_\theta(\mathbf{s}[n])^{\mathrm{T}}, \mathbf{h}_{\Delta\tau}(\mathbf{s}[n])^{\mathrm{T}}]^{\mathrm{T}}$, where

$$\begin{aligned}\mathbf{h}_\theta(\mathbf{s}[n]) &= [h_{\theta,1}(\mathbf{s}[n]), \ldots, h_{\theta,N_{\mathrm{RRH}}}(\mathbf{s}[n])]^{\mathrm{T}} \\ \mathbf{h}_{\Delta\tau}(\mathbf{s}[n]) &= [h_{\Delta\tau,1}(\mathbf{s}[n]), \ldots, h_{\Delta\tau,N_{\mathrm{RRH}}-1}(\mathbf{s}[n])]^{\mathrm{T}},\end{aligned} \tag{24}$$

with

$$\begin{aligned}h_{\theta,i}(\mathbf{s}[n]) &= \operatorname{acrtan}\left(\frac{y[n]-y_i}{x[n]-x_i}\right) \\ h_{\Delta\tau,j}(\mathbf{s}[n]) &= \frac{\Delta\mathbf{p}_j[n] - \Delta\mathbf{p}_{k_{\mathrm{REF}}}[n]}{c},\end{aligned} \tag{25}$$

where $\Delta\mathbf{p}_j[n] = \|\mathbf{p}[n] - \mathbf{p}_j\|$ is the distance between the train and the j^{th} RRH, $\Delta\mathbf{p}_{k_{\mathrm{REF}}}[n] = \|\mathbf{p}[n] - \mathbf{p}_{k_{\mathrm{REF}}}\|$ is the distance between the train and the reference RRH, and c is the speed of light. The obtained a priori mean and covariance estimates are then updated in the second stage of the EKF using the available measurements $\mathbf{y}[n]$ according to

$$\mathbf{K}[n] = \hat{\mathbf{P}}^-[n]\mathbf{H}[n]^{\mathrm{T}}\left(\mathbf{H}[n]\hat{\mathbf{P}}^-[n]\mathbf{H}[n]^{\mathrm{T}} + \mathbf{R}[n]\right)^{-1} \tag{26}$$

$$\hat{\mathbf{s}}^+[n] = \hat{\mathbf{s}}^-[n] + \mathbf{K}[n](\mathbf{y}[n] - \mathbf{h}(\hat{\mathbf{s}}^-[n])) \tag{27}$$

$$\hat{\mathbf{P}}^+[n] = (\mathbf{I} - \mathbf{K}[n]\mathbf{H}[n])\hat{\mathbf{P}}^-[n], \tag{28}$$

where $\mathbf{H}[n]$ is the Jacobian matrix of the considered non-linear measurement model function $\mathbf{h}(\cdot)$ evaluated at $\hat{\mathbf{s}}^-[n]$. Given the measurement model function, it is straightforward to show that entries of the Jacobian matrix $\mathbf{H}[n] = [\mathbf{H}_\theta[n], \mathbf{H}_{\Delta\tau}[n]]^{\mathrm{T}} \in \mathbb{R}^{(2N_{\mathrm{RRH}}-1)\times 4}$ in (26) can be written as

$$\mathbf{H}_\theta[n] = \begin{bmatrix} -\frac{\hat{y}^-[n]-y_1}{\|\hat{\mathbf{p}}^-[n]-\mathbf{p}_1\|^2} & \frac{\hat{x}^-[n]-x_1}{\|\hat{\mathbf{p}}^-[n]-\mathbf{p}_1\|^2} & \mathbf{0} \\ \vdots & \vdots & \vdots \\ -\frac{\hat{y}^-[n]-y_{N_{\mathrm{RRH}}}}{\|\hat{\mathbf{p}}^-[n]-\mathbf{p}_{N_{\mathrm{RRH}}}\|^2} & \frac{\hat{x}^-[n]-x_{N_{\mathrm{RRH}}}}{\|\hat{\mathbf{p}}^-[n]-\mathbf{p}_{N_{\mathrm{RRH}}}\|^2} & \mathbf{0} \end{bmatrix} \tag{29}$$

$$\mathbf{H}_{\Delta\tau}[n] = \begin{bmatrix} \eta^{(x)}_{\Delta\tau,1} & \eta^{(y)}_{\Delta\tau,1} & \mathbf{0} \\ \vdots & \vdots & \vdots \\ \eta^{(x)}_{\Delta\tau,N_{\mathrm{RRH}}-1} & \eta^{(y)}_{\Delta\tau,N_{\mathrm{RRH}}-1} & \mathbf{0} \end{bmatrix},$$

where

$$\begin{aligned}\eta^{(x)}_{\Delta\tau,i} &= \frac{\hat{x}^-[n]-x_i}{c\|\hat{\mathbf{p}}^-[n]-\mathbf{p}_i\|} - \frac{\hat{x}^-[n]-x_{k_{\mathrm{REF}}}}{c\|\hat{\mathbf{p}}^-[n]-\mathbf{p}_{k_{\mathrm{REF}}}\|}, \\ \eta^{(y)}_{\Delta\tau,i} &= \frac{\hat{y}^-[n]-y_i}{c\|\hat{\mathbf{p}}^-[n]-\mathbf{p}_i\|} - \frac{\hat{y}^-[n]-y_{k_{\mathrm{REF}}}}{c\|\hat{\mathbf{p}}^-[n]-\mathbf{p}_{k_{\mathrm{REF}}}\|}.\end{aligned} \tag{30}$$

Finally, the measurement noise covariance matrix $\mathbf{R}[n] = \mathrm{blkdiag}(\mathbf{R}_\theta[n], \mathbf{R}_{\Delta\tau}[n]) \in \mathbb{R}^{(2N_{\mathrm{RRH}}-1)\times(2N_{\mathrm{RRH}}-1)}$, where the AoA part is given as $\mathbf{R}_\theta[n] = \mathrm{diag}(\hat{\sigma}^2_{\theta,1}, \ldots, \hat{\sigma}^2_{\theta,N_{\mathrm{RRH}}})$, and the TDoA part $\mathbf{R}_{\Delta\tau}[n] = \hat{\sigma}^2_{\tau,k_{\mathrm{REF}}}\mathbf{I} + \mathrm{diag}(\hat{\sigma}^2_{\tau,1}, \ldots, \hat{\sigma}^2_{\tau,N_{\mathrm{RRH}}-1})$ is stemming from [16].

IV. Simulations and Result Analysis

The numerical evaluations in this paper are based on simulations on a real-life HST railway track between Beijing and Shanghai, China, where the track characteristics have been obtained from [12]. The simulation covers a travelled distance of approximately 73 km from Shanghai Hongqiao station to Suzhou North station, including a stop of 2 minutes at the Kunshan South station. The maximum velocity of the train is considered as 360 km/h, and the detailed train velocity for the whole track, including smooth acceleration characteristics, is shown in Fig. 3. Furthermore, the considered simulation parameters, including the model for the state-dependent variance of the angular velocity, are shown in Table I, where the channel related parameters are discussed in more detail in [14].

In Fig. 4, cumulative estimation errors over the whole track are shown for the train position, train velocity, and train heading, by considering the linear state-transition model, and the non-linear state-transition model with and without the state-dependent angular velocity variance, denoted as "static variance" and "dynamic variance" in Fig. 4, respectively. The results show that the positioning accuracy can be significantly improved with the non-linear state-transition model, and further improved by including the state-dependent angular velocity variance. Moreover, when considering the estimation accuracy of the train velocity and train heading, the non-linear state-transition model with the state-dependent angular velocity variance outperforms the other approaches. With the non-linear state-transition model and dynamic angular velocity variance, the 95 % percentiles of the estimation accuracies for the train position, train velocity, and train heading are 2.3 m, 0.47 m/s, and 1.6 deg, respectively. These are below the 3GPP-specified performance requirements, correspondingly given as 3 m, 2 m/s, and 2 deg, for the use case of machine control and transportation, as specified in [5, table 6.3.1].

In order to reveal the positioning performance for different HST mobility characteristics, in Fig. 5, cumulative error curves

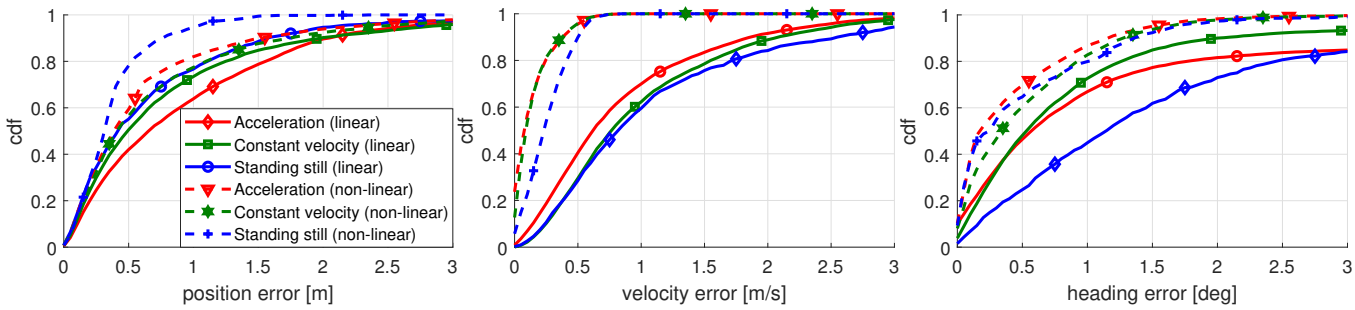

Fig. 5. Cumulative estimation errors for train position, train velocity, and train heading, with the linear state-transition model and the non-linear state-transition model over different mobility characteristics of the train.

for the train position, train velocity, and train heading, are shown separately for different mobility characteristics of the simulated track. Based on the shaded areas illustrated in Fig. 3, the track is divided into three categories, "acceleration", "constant velocity", and "standing still", from where the error statistics are shown for the approach with linear state-transition modeling and non-linear state-transition modeling with the state-dependent angular velocity variance. As seen in Fig. 5, the position error is significantly improved with the non-linear model, when the train is accelerating or standing still. However, when the train is cruising with a constant velocity, the performance difference is relatively small. However, by using the non-linear state-transition model, the velocity and heading estimation errors can be significantly reduced for all considered HST mobility characteristics. When the train is standing still, the linear state-transition model allows the train to turn around, whereas the non-linear model with the dynamic variance of angular velocity is able to restrict the turning rate.

V. Conclusion

In this paper, we studied positioning and tracking of HSTs in 5G NR system based on TDoA and AoA measurements with EKF-based positioning engine. In addition to traditional linear state-transition model of the EKF, we proposed and derived a non-linear state-transition model incorporated with the absolute train velocity and the train heading. Furthermore, we proposed using a dynamic state-dependent variance for the process noise regarding the angular velocity. Based on the characteristics of a real-life HST track, we performed simulations using specific 5G NR system parameterization according to guidelines specified by 3GPP. Although the focus of this paper was in HST scenario, the proposed model is applicable also to various other scenarios requiring high accuracy positioning and tracking, such as autonomous road vehicles, marine vessels, and solid wing aerial vehicles.

The simulation results showed that the positioning performance, including estimation of the train position, train velocity, and train heading, could be significantly improved by using the proposed non-linear state-transition model. Compared to the linear model, the non-linear model provided enhanced performance in all considered train mobility characteristics, especially when the train was standing still. The proposed approach achieved 95% percentile estimation errors of 2.3 m, 0.47 m/s, and 1.6 deg, for the train position, train velocity, and train heading, respectively, which meet the requirements for machine control and transportation use cases, specified by the 3GPP. Thus, the proposed positioning engine for 5G and beyond communication systems can be considered as an important facilitator of various mission critical services in future autonomous systems.

References

[1] R. Chen, W. Long, G. Mao, and C. Li, "Development trends of mobile communication systems for railways," *IEEE Commun. Surveys Tutorials*, vol. 20, no. 4, pp. 3131–3141, Fourthquarter 2018.

[2] F. Hasegawa *et al.*, "High-Speed Train Communications Standardization in 3GPP 5G NR," *IEEE Commun. Standards Mag.*, vol. 2, no. 1, pp. 44–52, Mar. 2018.

[3] "3GPP TR 38.913 v15.0.0 Study on Scenarios and Requirements for Next Generation Access Technologies (Rel. 15)," June 2018.

[4] "3GPP TSG RAN, RP-190752, New WID: NR Positioning Support," Mar. 2019.

[5] "3GPP TR 22.872 v16.1.0 Study on positioning use cases (Release 16)," Sept. 2018.

[6] J. Talvitie, T. Levanen, M. Koivisto, K. Pajukoski, M. Renfors, and M. Valkama, "Positioning of high-speed trains using 5G new radio synchronization signals," in *2018 IEEE Wireless Communications and Networking Conference (WCNC)*, April 2018, pp. 1–6.

[7] T. Levanen *et al.*, "Location-Aware 5G Communications and Doppler Compensation for High-Speed Train Networks," in *Proc. 2017 EuCNC*, June 2017, pp. 1–6.

[8] J. Talvitie *et al.*, "Positioning and Location-based Beamforming for High Speed Trains in 5G NR Networks," in *Proc. 2018 IEEE GLOBECOM Workshops*, Dec 2018, pp. 1–7.

[9] H. Wymeersch *et al.*, "5G mmWave Positioning for Vehicular Networks," *IEEE Wireless Commun.*, vol. 24, no. 6, pp. 80–86, Dec 2017.

[10] M. Koivisto *et al.*, "Joint Device Positioning and Clock Synchronization in 5G Ultra-Dense Networks," *IEEE Trans. Wireless Commun.*, vol. 16, no. 5, pp. 2866–2881, May 2017.

[11] X. Cui, T. A. Gulliver, J. Li, and H. Zhang, "Vehicle Positioning Using 5G Millimeter-Wave Systems," *IEEE Access*, vol. 4, pp. 6964–6973, 2016.

[12] OpenRailwayMap. [Online]. Available: www.openrailwaymap.org

[13] "3GPP TS 38.211 v15.3.0 NR Physical channels and modulation (Rel. 15)," Sept. 2018.

[14] "3GPP TR 38.901 v15.0.0 Study on channel model for frequencies from 0.5 to 100 GHz (Release 15)," June 2018.

[15] M. Roth, G. Hendeby, and F. Gustafsson, "EKF/UKF maneuvering target tracking using coordinated turn models with polar/Cartesian velocity," in *17th International Conference on Information Fusion (FUSION)*, July 2014, pp. 1–8.

[16] S. Sand, A. Dammann, and C. Mensing, *Positioning in Wireless Communications Systems*, 1st ed. Wiley Publishing, 2014.